Terrain Classification of Snow-Covered Watersheds

K. ELDER
Center for Remote Sensing and Environmental Optics
University of California Santa Barbara
Santa Barbara, California 93106, U.S.A.

R. E. DAVIS
U.S. Army Cold Regions Research and Engineering Laboratory
72 Lyme Road
Hanover, New Hampshire 03755-1290, U.S.A.

R. C. BALES
Department of Hydrology and Water Resources
University of Arizona
Tucson, Arizona 85221, U.S.A.

ABSTRACT

If the spatial distribution of snow can be estimated, it may be classified into areas, which may simplify snow melt calculations, melt water routing through the pack, and recovery of snow properties from remote sensing data. Complex topography produces spatially variable patterns of snow accumulation and ablation. Our objective in this study is to develop an automated method that unambiguously divides a snow-covered watershed into terrain units that: 1) do not overlap major subcatchment divides, 2) have similar net potential solar radiation within their boundaries, and 3) have relatively uniform snow water equivalence within their boundaries. It is shown that the number of classes delineated by this method will be orders of magnitude less than the number of nodes in a digital elevation model of even a small watershed, which can be on the order of 10^5 to 10^6. This method is developed in an alpine watershed whose landcover features are simple, it has little vegetation or soil cover. The method is suitable to distribute point energy balance calculations over a watershed.

INTRODUCTION

The topography of a watershed has a major impact on the distributions of the snow and the surface energy exchange. The distribution of snow in alpine areas is related to patterns of net solar radiation, but also depends strongly on processes that redistribute the snow (Elder et al., 1989, 1991). The distribution of snow within a basin is a necessary variable to improve energy and mass transfer models applied in snow covered areas because the distribution is irregular and the energy exchange rates are nonuniform. Solar radiation is a key factor in the surface energy exchange over alpine snow fields, and may be the dominant component (Zuzel and Cox, 1975). While the turbulent exchanges of sensible and latent heat may be important under some conditions, they are frequently of opposite sign during the melt season and almost always have fluxes of much lower magnitudes than radiation (Marks and Dozier, 1991). Thermal radiation is also lower in magnitude than the solar flux, and exhibits lower variation than the other components. Therefore, the topography is a primary factor controlling the spatial and temporal variations of snow metamorphism and melt.

There have been many approaches to using energy balance principles to predict snow pack condition and melt over a watershed, but we lack effective spatially-distributed snowmelt models capable of handling the complex terrain and providing process-level simulations (Dozier, 1987; Leavesley, 1989). Strategies to

reduce the computational complexity of this problem have segmented the terrain into a few simple units, such as elevation classes, then run a detailed simulation of the snow, or simplified the energy budget calculations, then run the simulation over many points, such as the nodes of a digital elevation model (DEM). In the first case the modeling approach assumes that the processes in the snow dominate over the terrain-controlled variations, while in the second case the converse is true. Much progress has been made recently in modeling the variation of solar radiation over complex terrain (e.g. Dubayah et al. 1990), and modeling the energy and mass balance of a snow cover at a point (e.g. Jordan, 1991). To take advantage of both these advances, we present a method to classify snow-covered terrain suitable for a distributed energy and mass transfer model.

This paper conceptually describes an image-based methodology to classify an alpine or non-forested watershed into terrain units, incorporating the accumulated effects of solar radiation and snow distribution. Our main objectives are to 1) model the seasonal patterns in accumulated net potential solar radiation in the visible and near-infrared wavelength regions, 2) identify a radiation accumulation period which best describes the potential variability of the thermal state of the snow pack before the onset of melt, 3) characterize the season-integrated distribution of snow cover, and 4) assess the superposition of radiation and snow cover patterns to form a classification.

The objective of this investigation is to classify an alpine watershed according to physical criteria into terrain units, and provide a realistic characterization of the terrain-induced variability. We also want to minimize the total number of terrain units because the number of calculation points for a detailed process-level snow model must be on the order of 10^2 for the problem to be tractable on large workstations. Therefore the number of terrain units must be orders of magnitude less than the number of grid nodes of the DEM used in generating the classification for even small to medium sized watersheds.

METHODS

Overview

This classification method is based on the spatial combination of two parameters, net potential snow accumulation and net potential radiation. Because of the large size of the data sets, and the availability of software to rapidly calculate terrain and radiation parameters, this work was carried out using the Image Processing Workbench (IPW), which is a UNIX-based image processing software system (Frew and Dozier, 1986; Frew, 1990). The data are stored as unsigned integer format as breakpoints, transformed from floating-point representation by a piecewise linear quantization. This convention reduces the storage required for images, and makes the software portable between machines with different internal floating-point representation. It also is the traditional representation of remotely-sensed image data.

Study Site

The test case for this study is the Emerald Lake watershed, a small alpine basin on the Marble Fork of the Kaweah River in Sequoia National Park, California. The Emerald Lake basin ($36°35' N$, $118°40' W$) comprises an area of approximately 120 ha, the total relief is 636 m, and the elevation ranges from 2780 m to 3416 m. The basin is a north-facing cirque, which is glacially scoured and flanked by cliffs on the south and west margins (Figure 1). The basin is represented in this study by a DEM with 48048 points, 5-m grid spacing, and vertical accuracy of better than 1 m. The DEM is treated as a single-band image by IPW. Topographic variables required to model the radiation are calculated at every DEM node and include slope and azimuth, horizons, and a sky view factor. Figure 2 shows a masked slope image of the Emerald Lake basin.

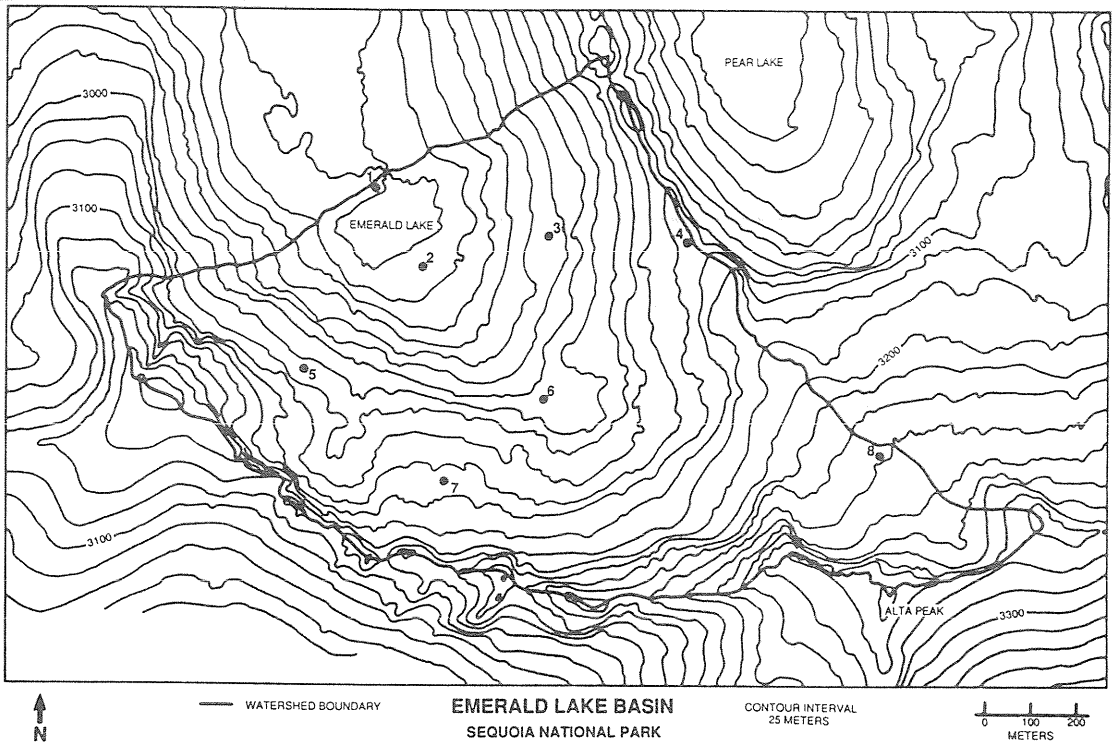

Figure 1. Topographic map of the Emerald Lake Basin, California. Numbered points show typical locations of snow pits.

Field Methods

The patterns of snow accumulation were surveyed over three years for this study. The survey technique involved measuring snow densities from snow pits and measuring snow depths with portable depth probes. Profiles of density measurements were obtained from the walls of snowpits by measuring the mass of 1-liter cuts, sampled vertically every 0.1 m. Average densities were calculated from several pits throughout the basin, and depth probes were then used with the average density interpolate SWE between the pit sites. The sites were randomly located on a 25-m grid registered to the a 5-m resolution DEM of the basin. Figure 1 shows an example of the points of a typical survey.

Incoming solar radiation was measured with hemispheric pyranometers at two sites, on a ridge at the watershed boundary and near the outlet of Emerald Lake. These measurements were used to check and adjust estimates of the clear sky solar radiation.

Net Potential Snow Accumulation

The net potential snow accumulation is an index parameter of the spatial heterogeneity of snow water equivalence (SWE). It is the amount of snow that will tend to accumulate in a local area relative to a larger-scale average. This parameter can take the form of a single-valued weight or a probability distribution function depending of the spatial density and temporal frequency of the data. The assumptions behind this parameter are that the annual patterns of local snow surplus and snow deficit are about the same year after year, and the relative difference between them is based on the mean SWE (Elder et al., 1991).

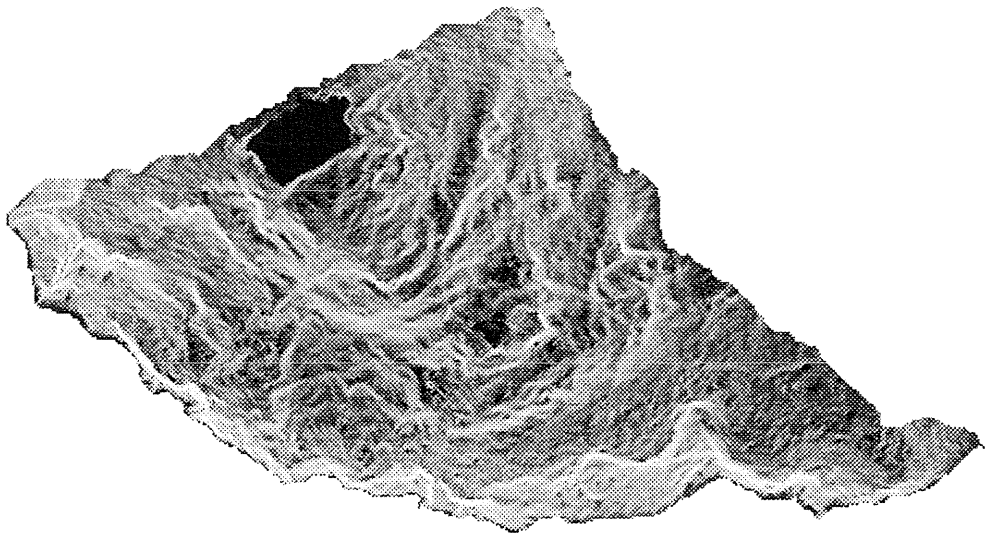

Figure 2. Masked slope image of the Emerald Lake Basin, California. Dark shades show low slopes and light shades show steep slopes.

A single-value form of the index of snow accumulation I_{SWE} is obtained at each of the points surveyed:

$$I_{SWE} \equiv \frac{SWE_i}{\overline{SWE'}} \tag{1}$$

where the point measurements SWE_i in an elevation zone are used to calculate the local mean for the elevation zone $\overline{SWE'}$:

$$\overline{SWE'} = \sum_{1}^{i} SWE_i \; A_i \tag{2}$$

A_i is the fraction of the zone area represented by the value SWE_i.

Net Potential Solar Radiation.

The net potential solar radiation is the clear-sky net solar radiation (accumulated) over the period of interest. The assumption in using this parameter in the classification is that it is the most sensitive indicator of snow pack regions with different thermal conditions, which is supported by Zuzal and Cox (1975) and Marks (1991). We calculate the net potential solar radiation accumulated for a period that yields the maximum range distributed over the watershed while there is still continuous snow cover.

The values for molecular absorption in the atmosphere under clear-sky conditions over the test area were estimated from the LOWTRAN7 model (Kneizys et al., 1988) and used for input to a two-stream approximation to the radiative transfer equation to obtain total downwelling radiation, and the diffuse and direct components, by wavelength (Meador and Weaver, 1980):

$$\frac{dF\uparrow(\tau)}{d\tau} = \gamma_1 F\uparrow(\tau) - \gamma_2 F\downarrow(\tau) - \gamma_3 \omega_0 S_0 e^{-\tau/\mu_0} \tag{3a}$$

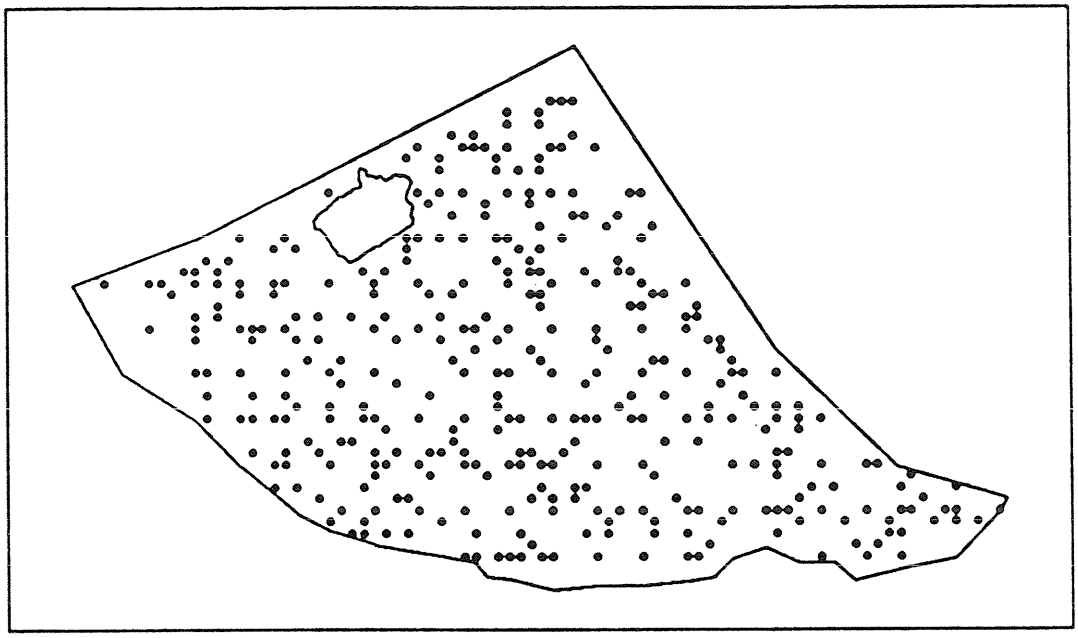

Figure 3. Example of survey points in an outline of Emerald Lake Basin, California.

$$\frac{dF_{\downarrow}(\tau)}{d\tau} = \gamma_2 F_{\uparrow}(\tau) - \gamma_1 F_{\downarrow}(\tau) + \gamma_4 \omega_0 S_0 e^{-\tau/\mu_0} \tag{3b}$$

The upward and downward fluxes are $F_{\uparrow}$ and $F_{\downarrow}$ respectively, S_0 is the exoatmospheric parallel-beam flux, incident at angle arcos μ_0, ω_0 is the single-scattering albedo (i.e. the ratio of extinction by scattering to total extinction), and the γ-values parameterize the scattering phase function. The optical depth coordinate is τ, and the Mie equations are used to calculate the single scattering albedo ω_0 and the scattering asymmetry parameter g. The γ values parametrize the scattering phase function and are obtained from g, ω_0, and μ_0 (Meador and Weaver, 1980). The boundary conditions used for the solution two-stream equations are that $F_{\downarrow}(0) = 0$ at the top, and the lower boundary τ_0 is a diffuse reflector whose reflectance is R_0: For a level surface

$$F_{\uparrow}(\tau_0) = R_0 \left[F_{\downarrow}(\tau_0) + \mu_0 S_0 e^{-\tau_0/\mu_0} \right] \tag{4}$$

The directional hemispheric transmittance, T_s, is equivalent to what is measured with a level hemispheric pyranometer.

$$T_s \equiv \frac{F_{\downarrow}(\tau_0) + \mu_0 S_0 e^{-\tau_0/\mu_0}}{\mu_0 S_0} \tag{5}$$

From these boundary conditions and suitable estimates of the input parameters the two-stream equations can be solved. Visibility was used as an adjustable parameter and the calculations were iterated until T_s matched clear sky pyranometer readings from the basin. More complete descriptions and solutions to the two-stream equations can be found in Dozier (1980) and Dubayah et al. (1990).

The direct irradiance and diffuse irradiance must be calculated, once the transmittance T_s is obtained, to calculate the potential incoming solar radiation extended over the terrain. The direct irradiance on a slope is $\mu_s S_0 e^{-\tau_0/\mu_0}$, where μ_0 is the cosine of the solar illumination angle, θ_0, on a horizontal surface and μ_s is the cosine of the solar illumination angle on the slope (Sellers, 1965),

$$\mu_s = \cos\theta_0 \cos S + \sin\theta_0 \sin S \cos(\phi_0 - A) \quad (6)$$

The solar azimuth is ϕ_0. The sine of the slope angle S and the slope's azimuth A, are stored in a two-band IPW image as linear quantizations (Dozier and Frew, 1990).

The diffuse irradiance is calculated as the product of the downward diffuse irradiance and the sky-view factor V_d, which is the ratio of the diffuse sky irradiance at a point in the terrain and that on an unobstructed horizontal surface:

$$V_d = \frac{1}{2\pi} \int_0^{2\pi} [\cos S \sin^2 H_\phi + \sin S \cos(\phi - A)(H_\phi - \sin H_\phi \cos H_\phi)] \, d\phi \quad (7)$$

H_ϕ is the horizon parameter, the angle from zenith to the local horizon at a specified azimuth, and is calculated according to Dozier and Frew (1990). The contributed irradiance reflected from the surrounding terrain is also calculated using an algorithm described by Dozier and Frew (1990).

The net solar radiation is the incoming radiation minus the reflected radiation integrated over the wavelengths 0.35 – 3.0 μm. Calculation of the detailed spectral integral for all of the points in the basin is too time consuming, so the albedo of the snow is parameterized into two bands, short wave, (0.35 – 0.8 μm), and near-infrared, (0.8 – 3.0 μm) based on Marshall and Warren (1987), and the spectral downwelling radiation to is integrated get total downwelling radiation in the two bands.

The distribution of net solar radiation is calculated as average daily values which are accumulated and normalized over various periods from December to spring. Different accumulation periods are simulated and displayed while the user interactively chooses the period where the maximum contrast is produced in radiation distributed across the test area. We reduce the number of bits used to display the data as a brute-force method to generalize radiation classes.

Classification Algorithm

The images for the two parameters, net potential snow accumulation and net potential solar radiation, are combined in a band-interleave process to form a two-band IPW image. In this case each sample in the line-and-sample format represents a vector consisting of the two parameters. The unique combinations of single-valued areas of both parameters form the terrain-unit classes. The corresponding values of net potential snow accumulation and net potential radiation from a random sample of 1000 location within the basin were clustered to identify the statisitcs of similar groups within the basin. The terrain unit classifications were then obtained with a Bayesian classifier based on the structure of similar groups obtained from the clustered subimages (Richards, 1986). The user then adjusts the number of classes of each parameter to obtain a trial classification.

RESULTS

The net potential snow accumulation was calculated from the spatial distributions of point measurements for three snow seasons. Table 1 shows the results of point measurements of I_{SWE} at maximum snow accumulation for the period of study.

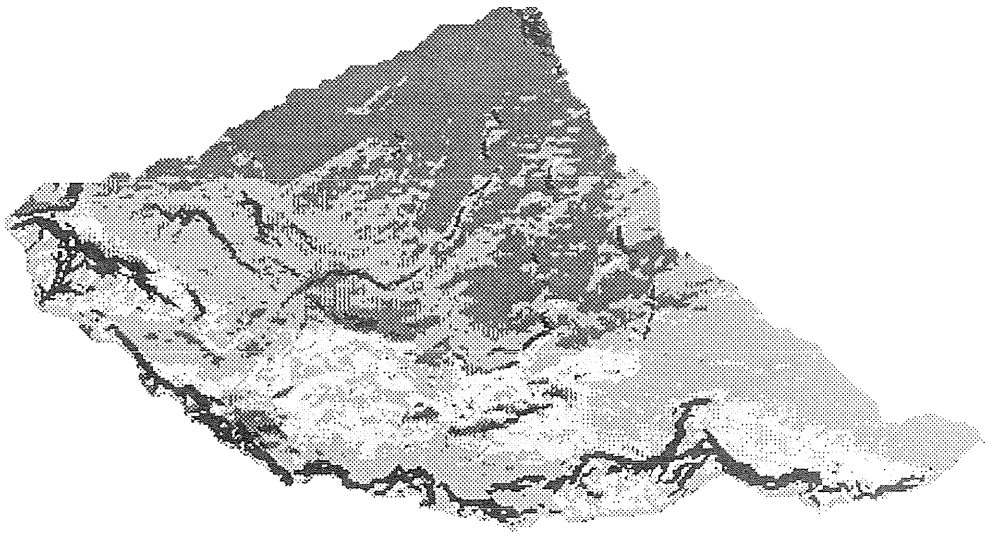

Figure 4. Classification of the net potential accumulation of snow, shown in a masked image of Emerald Lake Basin, California.

Table 1. Summary of Seasonal Snow Characteristics

Year	n	$\overline{SWE}$ (m)	SWE_T (m^3)	Standard Error of Mean (m^3)	Coefficient Variation
1986	86	2.00	2,398,560	7,124	33.1
1987	256	0.598	718,300	2,860	62.3
1988	354	0.630	750,700	2,652	62.8

The parameter SWE_T is the estimate of the total basin SWE. The snow survey methodology was refined for the years 1987 and 1988, and this is reflected in the greater number of samples for those years. Figure 4 shows the composite results of the snow classification, displayed as five normalized classes, dark represents areas likely to experience snow deficits and light areas represent areas likely to experience areas of snow surplus. For example, the light colored areas along the base of the cliffs at the higher perimeter of the basin (see Figure 1) represent large snow accumulations which form from sloughing of snow from the cliffs.

When large sample sizes are obtained, as in this work, an accurate estimate of basin SWE volume can be obtained by taking the arithmetic mean of all the point SWE estimates. Using the standard error of the mean as an indicator of our ability to estimate the true sample mean, we found that the SE was less than 4% of the mean for surveys around the date of peak accumulation in 1987 and 1988. This result shows that we do not cause large errors in the estimates of total SWE by the classification, which looses some detail in the variability of SWE. The SE was about somewhat higher in 1986, because of the fewer number of points, and the large accumulations of snow. The standard deviation is high, indicating that the spatial variability of the SWE estimates is high, shown by the coefficients of variation of about 60%.

The radiation data was accumulated for the period December through March, which provided the greatest variation in net potential solar radiation. Figure 5 shows the classification map for accumulated net potential radiation December through March, displayed as five classes.

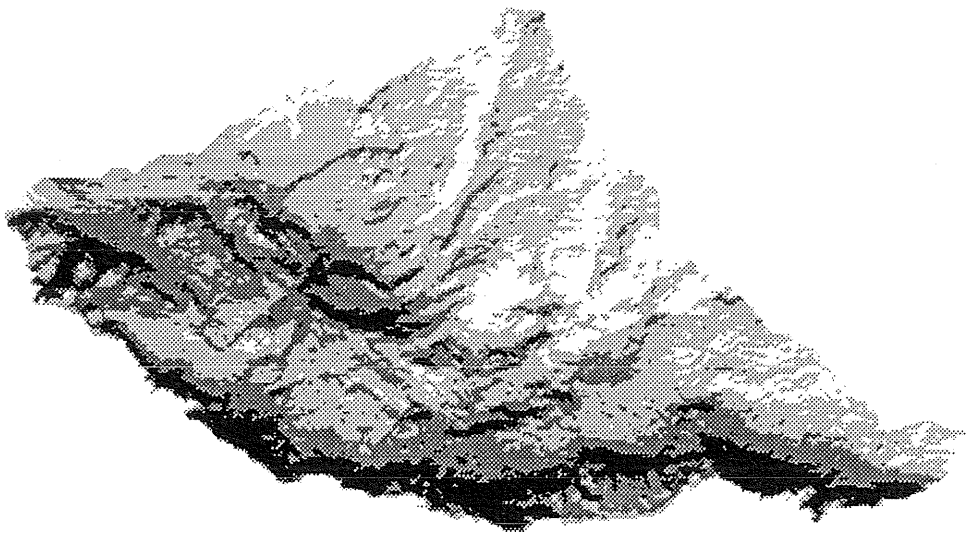

Figure 5. Classification of the net potential solar radiation, shown in a masked image of Emerald Lake Basin, California.

Shorter accumulation periods were characterized by lower overall levels of net potential radiation and lower variation. Higher levels of net potential radiation and lower variation was exhibited in longer periods of accumulation. Therefore this accumulation period not only provides the largest spatial variation, but also a balance between low and high levels.

An image of the patterns produced by the composite classification is shown in Figure 6. The terrain units on this image represent generalized areas which have an optimized likelihood of similar net radiation and similar snow water equivalence. The total number of different classes is less than 25, and the number of individual areas is less than 300.

SUMMARY

We have described the conceptual methodology to divide an alpine watershed into terrain units which have similar snow water equivalent and similar net potential solar radiation. This methodology has been illustrated with an example alpine watershed in the Sierra Nevada of California. In our example, the classification has produced a few hundred terrain units, which is orders of magnitude less than the number of nodes of the digital elevation model used to produce it. While the radiation modeling can be carried out in the laboratory, the accurate determination of the snow accumulation index requires extensive field measurements over a few winter and spring seasons. We anticipate the patterns produced by this classification to be reasonable, except in seasons with extreme events such as very low snow, or exceptionally large storms, which may mask the average patterns of variation. The most pressing application for our further research is to use this method to distribute an energy and mass transfer model of an alpine snow pack and simulate snow melt runoff. Another application is to use this classification to guide selection of reference snow courses in an alpine watershed. In addition, we suggest that the patterns produced by the classification could have close correspondence with patterns observed on remote sensing imagery of reflectance from snow in complex terrain.

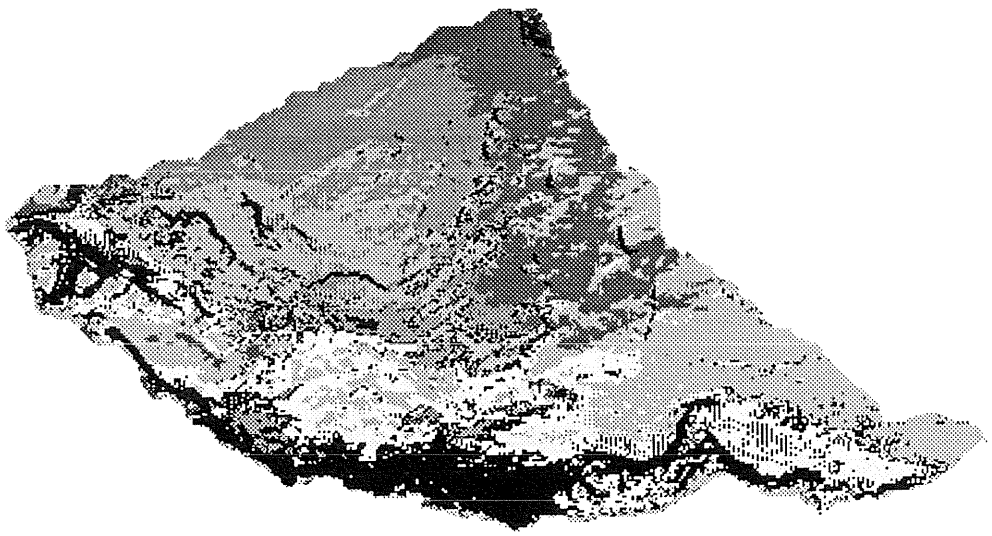

Figure 6. Terrain unit classification of the combination of net potential radiation and net potential snow accumulation for Emerald Lake Basin, California.

TESTS AND APPLICATIONS

To evaluate the utility of this classification scheme, we plan to distribute a detailed snow energy and mass transfer model to calculate snow melting and runoff production at the snow pack base. This model will be implemented assuming that the centers of the terrain units are representative of the area within the boundaries, using slope and azimuth parameters aggregated from the area within each unit. The SWE for each unit will be estimated using the the SWE index weight and a measurement of SWE from a few reference snow courses. It is possible that the computational complexity might be further reduced by combining nearby terrain units into one class for energy balance simulations, then distributing the results according to location. The actual net solar radiation will be derived from pyranometer measurements, estimates of the snow surface grain size, and radiation index weights. The one-dimensional model does not simulate the three dimensional flow of water through inclined snow covers. However, we expect rapid hydrologic response of the basin and subcatchments because of the steep slopes and lack of appreciable soil. Therefore the time sequence of melt volumes arriving at the base of the pack can be compared with runoff volumes at each of the stream inlets at daily and weekly time scales to provide a suitable basis for assessing the classification performance.

The classification procedure delineates patterns of areas assumed to have approximately equal snow cover and similar net potential solar radiation. This implies that each class represents snow with a similar thermal and metamorphic state, except in areas where turbulent energy exchange dominates the energy balance. If this is the case, we would expect similar patterns in remote sensing imagery in spectral regions where the signal is sensitive to the physical properties of the snow. For example, these areas should be expressed as areas of similar albedo in the visible and near-infrared spectral region, especially in the near-infrared wavelengths. This would be manifested as patterns of the optically equivalent grain size. The distribution of spectral reflectance from snow in the near-infrared wavelengths is anisotropic, and recent progress has been made in modeling the bidirectional reflectance distribution function of snow

(e.g. Dozier et al., 1988). Therefore, if images with high spectral resolution were registered to the DEM so that the anisotropy of reflectance could be deconvolved from the problem, maps of grain size could be synthesized and compared with the patterns of the classification.

ACKNOWLEDGEMENTS

Research support was provided by the California Air Resources Board, the University of California Water Resources Center, the NASA EOS program and by the U.S. Army Corps of Engineers. A great deal of software support was provided by Jim Frew at the Center for Remote Sensing and Environmental Optics, University of California Santa Barbara. Jeff Dozier of the NASA EOS Program and the Center for Remote Sensing and Environmental Optics, University of California Santa Barbara, provided the ideas and algorithms for the radiation modeling.

REFERENCES

Dozier, J. (1980) A clear-sky spectral solar radiation model for snow-covered mountainous terrain, *Water Resources Research, 16,* 709-718.

Dozier, J. (1987) Recent research in snow hydrology. *Reviews of Geophysics, 25* (2), 153-161.

Dozier, J., R. E. Davis, and A. W. Nolin (1988) The spectral bidirectional reflectance of snow *Spectral Signatures of Objects in Remote Sensing,* Fourth International Colloquium, ESA SP-287, European Space Agency, 87-92.

Dozier, J. and J. Frew (1990) Rapid calculation of terrain parameters for radiation modeling from digital elevation data, *IEEE Transactions on Geoscience and Remote Sensing, GE28(5),* 963-969.

Dubayah, R., J. Dozier & F. W. Davis (1990) Topographic distribution of clear-sky radiation over the Konza Prairie, Kansas. *Water Resources Research 26* (4), 679-690.

Elder, K., J. Dozier & J. Michaelsen (1989) Spatial and temporal variation of net snow accumulation in a small alpine watershed, Emerald Lake basin, Sierra Nevada, California, U.S.A. *Annals of Glaciology, 13,* 56-63.

Elder, K., J. Dozier & J. Michaelsen (1989) Snow accumulation and distribution in an alpine watershed, *Water Resources Research, 27(7),* 1541-1552.

Frew, J. and J. Dozier (1986) The Image Processing Workbench: portable software for remote sensing instruction and research, *Proceedings IGARSS '86, ESA SP-254,* 271-276.

Frew, J. (1990) The Image Processing Workbench, PhD Dissertation, Department of Geography, University of California, Santa Barbara.

Jordan, R. (1991) A one-dimensional temperature model for a snow cover: technical documentation for SNTHERM.89, U.S. Army Cold Regions Research and Engineering Laboratory, Special Report 657.

Kneizys, F. X., E. P. Shettle, L. W. Abreu, J. H. Chetwynd, G. P. Anderson, W. O. Gallery, J. E. A. Selby, and S. A. Clough (1988) Users Guide to LOWTRAN7 *Report AFGL-TR-88-0177,* Air Force Geophysics Laboratory Bedford, MA.

Leavesley. G. H. (1989) Problems of snowmelt runoff modelling for a variety of physiographic and climatic conditions, *Journal of Hydrologic Sciences, 34(6)* 617-634.

Marshall, S. E. and S. G. Warren (1987) Parameterization of snow albedo for climate models, Large Scale Effects of Seasonal Snow Cover, *IAHS Publication No. 166,* International Association of Hydrological Sciences, Wallingford, UK, Eds. B. E. Goodison, R. G. Barry, and J. Dozier, 43-50.

Meador W. E. and W. R. Weaver (1980) Two-stream approximations to radiative transfer in planetary atmospheres: a unified description of existing methods and a new improvement, *Journal of the Atmospheric Sciences, 37(3)* 630-643.

Richards, J. A. (1986) *Remote Sensing Digital Image Analysis,* Springer-Verlag, New York.

Sellers, W. D. (1965) *Physical Climatology,* University of Chicago Press, Chicago.

Zuzel, J. F., and L. M. Cox (1975) Relative importance of meteorological variables in snowmelt, *Water Resources Research, 11,* 174-176.